



Exploring the kinetics of Ordered Silicon Nanowires with the Formation of Nanogaps Using Metal-assisted Chemical Etching

Journal:	<i>Physical Chemistry Chemical Physics</i>
Manuscript ID:	CP-COM-09-2014-004237.R2
Article Type:	Communication
Date Submitted by the Author:	29-Oct-2014
Complete List of Authors:	Chen, Chia-Yun; National Chi Nan University, Department of Applied Materials and Optoelectronic Engineering Liu, Yu-Rui; National Chi Nan University, Department of Applied Materials and Optoelectronic Engineering

SCHOLARONE™
Manuscripts

Cite this: DOI: 10.1039/c0xx00000x

www.rsc.org/xxxxxx

ARTICLE TYPE

Exploring the kinetics of Ordered Silicon Nanowires with the Formation of Nanogaps Using Metal-assisted Chemical Etching

Chia-Yun Chen,* and Yu-Rui Liu

Received (in XXX, XXX) Xth XXXXXXXXXX 20XX, Accepted Xth XXXXXXXXXX 20XX

DOI: 10.1039/b000000x

Actual dimension control of silicon (Si) nanowire arrays was conducted using metal-assisted chemical etching on Si patterned by electron beam lithography. The appearance of nanogaps at the edge of each nanowire provides the diffusion pathways of reactants for Si dissolution, predominantly causing distinct etching rates that depend on the spacings of nanogaps.

Silicon (Si) nanowires with one-dimensionality and nanoscale features were intensively studied for various applications, such as solid-state electronics^{1,2}, energy conversion³, and optoelectronic⁴ and photonic^{5,6} devices. In designing Si nanowires for practical devices, controllability over localizations and dimensions has been observed to be particularly essential⁷. Moreover, assembling the Si nanowires in an ordered and aligned configuration can further enable them to exhibit collectively the material characteristics and properties of effective media, which are especially applicable in the practical development of miniaturized devices and even in the manufacture of commercial products⁸. In this study, we utilized metal-assisted chemical etching (MaCE) on patterned Si to tune the geometries of nanowire arrays accurately^{9–12} and to satisfy the aforementioned specific criteria. Patterning of Si was accomplished by standard electron beam lithography (EBL) for independently modulating the geometric factors of metal catalysts. In contrast to other patterning techniques, such as lithography assisted with nanosphere¹³, block copolymer¹⁴, and anodic aluminum oxide¹⁵ templates, where the defined patterns are inevitably bound with template structures, the present design strategy is unlimited in terms of pattern shapes and locations and further allows the feasibility of decoupling each geometric parameter. More importantly, systematic explorations of etching kinetics were conducted, which provide the basis for the quantitative assessment of the correlation between catalyst area and etching rates.

Department of Applied Materials and Optoelectronic Engineering, National Chi Nan University, Nantou 545, Taiwan. Email: timychen@ncnu.edu.tw

† Electronic supplementary information (ESI) available: Supporting figures discussed in the main text are included.

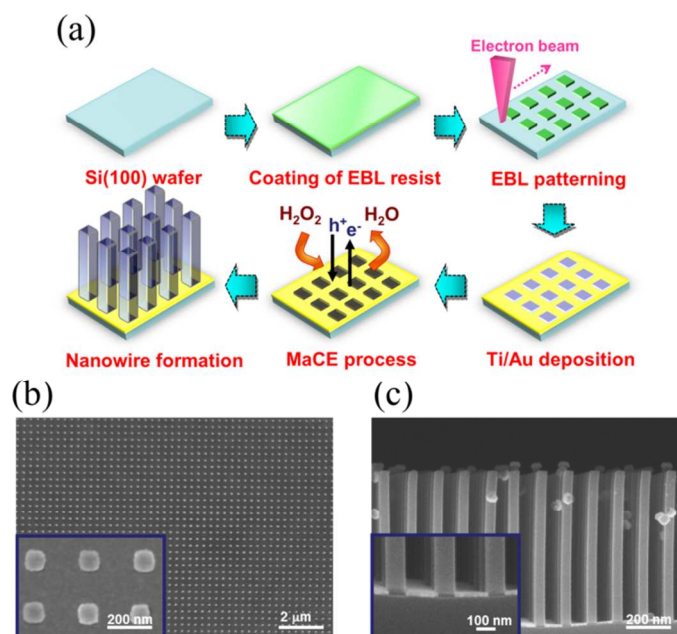


Fig. 1. (a) Schematic illustrations of process flow for synthesizing Si nanowire arrays with accurately tuned geometries. (b) Top-view SEM image of lithographic patterns after Ti/Au deposition. Regulated metal meshes with square-shaped arrays can be observed in the inset figure. (c) Cross-sectional SEM image of the as-prepared Si nanowire arrays. The inset figure clearly indicates that the metal meshes maintain similar sizes and shapes after the 5 min MaCE process.

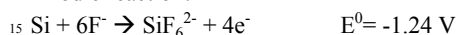
Fig. 1(a) shows the schematic process flow for the formation of ordered Si nanowire arrays with tuned feature dimensions. In general, nanowire patterns were defined by the EBL process, followed by metal deposition. First, a 200 nm-thick layer of PMMA resists (950 K) was spin-coated onto pre-cleaned Si substrates (5,000 rpm, 30 s) and subsequently merged in the sequential soft-bake treatments (180 °C, 2 h). Then, the exposed PMMA resists were subjected to the e-beam writing process, followed by the developing process (1:3 of MIBK/IPA developer). Next, 3 nm-thick adhesive Ti and 20 nm-thick Au layers were uniformly deposited using an electron gun evaporator. The resulting patterns are shown in Fig. 1(b), where the diameter and pitch size of remnant resists are 85 nm and 140 nm, respectively, with size deviation less

than 4 nm, and exhibit a square shape at each dot. Subsequently, we conducted the lift-off process to transfer our designed patterns onto the Si substrates. The sample size for each structure with tuned dimensions is $50\ \mu\text{m} \times 1,000\ \mu\text{m}$. Finally, to construct Si nanostructures with defined features, the MaCE process was readily conducted on these Ti/Au nanopatterns, as depicted in Fig. 1(a). Si etching experiments were conducted by immersing the patterned Si in the mixed solutions containing 0.9 M of H_2O_2 and 4.5 M of HF for 1 min to 10 min at room temperature. The involved electrochemical reactions can be expressed by the following equations^{16,17}:

Cathodic reaction:



Anodic reaction:



Such catalytic etching is initiated with hole injections from H_2O_2 oxidants because the reduction potential of H_2O_2 is higher than the valence band of Si. Moreover, Ti/Au metal meshes behave as the microscopic cathodes that enable the electrochemical oxidation of Si beneath them. Then, the oxidized Si was chemically dissolved using HF etchants, allowing the newly exposed Si to come in contact with the metal catalysts, which further facilitated the next cycle of electrochemical–chemical series reactions. Notably, charge transport is accompanied by the effective contact of H_2O_2 /HF reactants with the Au/Si interfaces¹⁸, which remarkably affects the etching kinetics on patterned Si at the nanoscale. This phenomenon will be further discussed later. Fig. 1(c) shows the cross-sectional scanning electron microscopy (SEM) images of etched nanowire arrays. Some residual PMMA resistance along with metal catalysts can be observed because of the uncompleted lift-off process, but the fabricated Si nanowires are explicitly uniform in morphology. Notably, the dynamically stable movement of Au meshes during dissolution of Si results in etched nanowires with particularly smooth sidewalls^{14,15}, which facilitates the development of Si-based optics by preventing the undesired scattering of propagation light¹⁹. These findings can be further supported by observing the metal meshes after the lengthy etching process, as shown in the inset of Fig. 1(c). The shapes and dimensions of catalyst nanopatterns are preserved at the bottom side of etched nanowires after a 5 min reaction.

By combining the EBL patterning technique with the MaCE process, the precise tunability of nanowire dimensions is achievable, as shown in Fig. 2. In this study, we independently modulated the pitch size of nanopatterns from 230 nm to 170 nm and 140 nm to analyze the dependence of etching kinetics on the geometric spacings of ordered nanopatterns. As such, three different pitch sizes of EBL patterns were predefined on a single Si(100) substrate, with a fixed distance of $100\ \mu\text{m}$ between each designed pattern. The underlying fabrication strategy is to ensure that consistent etching conditions can be achieved at different patterns, including the concentrations of reactants, environmental temperature, and reaction time. Accordingly, the morphologies of etching results are shown in Fig. 2. Although an approximately similar diameter of nanowires (85 nm) from

three designed patterns can be observed [Figs. 2(a) to 2(c)], the nanowire length apparently increases with the reduction in pitch size, as shown in Figs. 2(d) to 2(f). Moreover, quantitative examinations of pitch size after the 8 min etching process are shown in Fig. 3(a). The mean spacing of nanowires for the three designed patterns is 228 nm, 168 nm, and 136 nm, with size deviation less than 5 nm, as shown in the inset of Fig. 3(a).

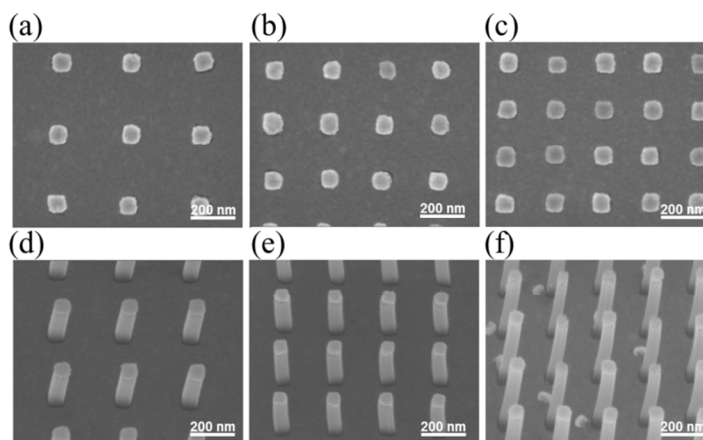
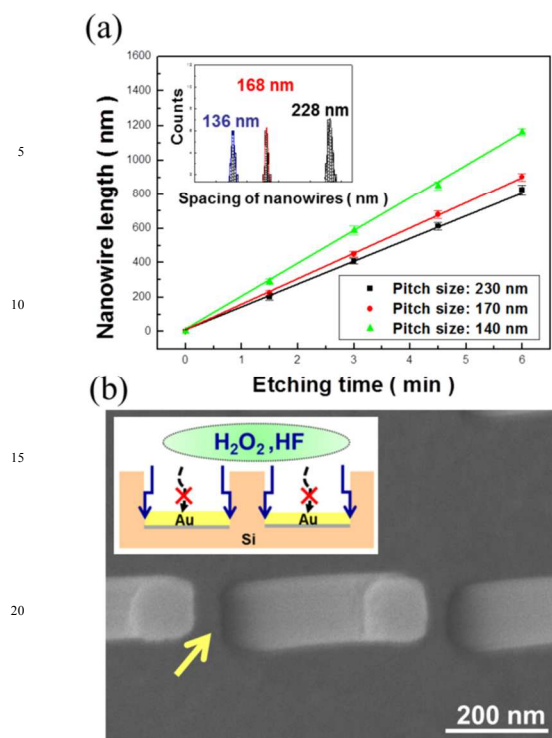


Fig. 2. Top-view SEM images of formed nanowire arrays obtained from (a) pitch size = 230 nm, (b) pitch size = 170 nm, and (c) pitch size = 140 nm. (e) and (f) 30° tilt-view SEM images of the corresponding nanowire arrays.

These features validated the finding that the combination of EBL patterning technique with Au-assisted catalytic etching shows actual tenability of dimensions for the Si etching technique in the sub-100 nm level. Moreover, the formation rates of all modulated nanowire arrays show the controllability of their lengths, in which the nanowire lengths linearly increase with the increase in etching time, as shown in Fig. 3(a). In addition, the formation rate of nanowires on patterned arrays with 140 nm pitch is approximately 1.1 and 1.6 times higher than that on patterned arrays with 170 nm and 230 nm pitch, respectively. These geometry effects have recently been discussed using the one-step MaCE process²⁰, but rarely reported using the H_2O_2 /HF-based two-step MaCE method. Fig. 3(b) shows the high-magnification SEM image of etched nanowires. At the edge of each nanowire, we can clearly observe the existence of nanogaps located between the formed nanowires and surrounding metal meshes. The width of these nanogaps is normally 4 nm to 7 nm. These nanogaps appear in conjunction with every etched nanowire. Their widths and geometries remain unchanged regardless of etching time (1 min to 5 min), as shown in the Electronic Supplementary Information. The consistent size of nanogaps explicitly implies the fact that these nanogaps do not result from side etching during the MaCE process.



25 Fig. 3. (a) Plot of etching time with respect to the length of
 30 nanowire arrays obtained from catalyst patterns with three
 different pitch sizes. The inset figure shows the corresponding
 statistical distributions of nanowire spacings. (b) High-
 magnification SEM image of etched nanowires. A nanogap
 appears at the edge of an etched nanowire, as denoted by a yellow
 arrow. The inset figures further visualize the reaction pathway of
 active reactants with Si.

Based on these findings, we speculated that these periodic
 gaps serve as the effective pathways that allow aqueous
 reactants to come in contact with metal catalyst-covered Si.
 The Au films used in this study are substantially thick and
 behave as a continuous layer, which, therefore, inhibits the
 direct penetration of aqueous reactants to metal catalyst-
 covered Si, as illustrated in the inset of Fig. 3(b). The top-
 view SEM image of deposited Ti/Au films prior to conducting
 the MaCE process is also shown in the Electronic
 Supplementary Information. Moreover, the holes generated by
 H_2O_2 oxidants are preferentially consumed at the metal/Si
 interfaces because of the lower Schottky barrier of hole
 injections toward Si. These features create the concentration
 gradients of holes that drive more H_2O_2 reactants to diffuse
 horizontally beneath metal catalysts, rather than occurring at
 the edge of catalyst films solely until the complete removal of
 oxidized Si at interfaces. These reactions lead to the
 homogeneous distribution of holes in Si underneath Au films,
 resulting in the uniform vertical movement of metal meshes
 sinking into Si.

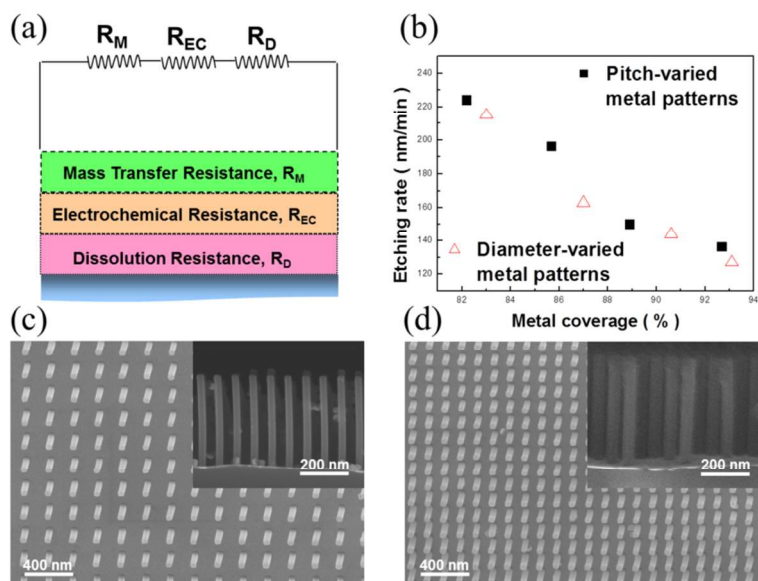


Fig. 4. (a) Evolution of etching kinetics using the
 phenomenological series resistance model. (b) Relationship
 between the area of metal coverage and etching rates. Data
 are obtained by independently varying the pitch sizes and
 diameters of metal patterns prior to the MaCE process. A
 representative SEM image of the prepared nanowire arrays
 with (c) sparse and (d) dense distributions. The correspond-
 ing cross-sectional SEM images of nanowire arrays are
 shown in the inset figures..

On the basis of measured etching rates on patterned Si,
 the phenomenological model²¹ can be applied to elucidate
 this geometry effect on catalytic etching of Si, as shown in
 Fig. 4(a). In this model, the electrochemical oxidation of Si
 and the chemical dissolution of oxidized Si constitute the
 essential steps for determining the kinetics of the etching
 process, reflecting the kinetic resistances in series with
 R_{EC} and R_D , respectively, which are consistent with
 previous studies^{21,22}. However, combined with the contribu-
 tions from R_{EC} and R_D , an additional effect, R_M ,
 provides appreciable resistance through the transport of
 reactants before reaching the metal/Si interfaces. Given that
 all the metal patterns encounter a similar etching environ-
 ment, that is, R_{EC} and R_D are approximately identical in
 all cases, R_M is considered the dominant factor that
 diversifies the etching kinetics. Specifically, with larger
 spatial pitch size of metal meshes, R_M increases because
 of the decrease in the numbers of nanogap arrays support-
 ing the diffusion pathways of reactants reaching the Si,
 leading to the suppression of Si dissolution. Meanwhile,
 the coverage area of metal meshes is increased correspond-
 ingly, which inevitably induces the active reactants to
 travel farther to remove Si at interfaces completely. These
 combined effects slow down the entire dynamic process,
 and the extent of deceleration is readily modulated by the
 metal coverage area.

We independently modulated the pitch size (P) and diameter
 (D) of nanopatterns to analyze the universal influences of
 metal coverage on Si etching. A similar MaCE process was
 conducted on these pitch-varied and diameter-varied Au
 meshes deposited

on Si, as shown in Fig. 4(b). In this study, the ratio of Ti/Au metal coverage with the same thickness is estimated using the following equation:

[Area of metal coverage / (Area of metal coverage + Area of exposed Si)] x 100%

The measured etching rates were recorded and plotted with respect to the ratio of metal coverage, where an explicit correlation can be clearly observed. The spatial ordering of patterned metal is required to allow decoupling of the geometry effects and to analyze further the general influences on etching kinetics. Accordingly, two representative diversified nanowire arrays in terms of metal coverage are also investigated, where sparse nanowires ($P = 170$ nm, $D = 60$ nm, and metal coverage = 93%) have shorter nanowire lengths than dense nanowires ($P = 85$ nm, $D = 85$ nm, and metal coverage = 75%), as separately shown in Figs. 4(c) and 4(d). Such kinetic evolution clearly illustrates the rule of catalyst geometry on the kinetic dissolution of Si via the MaCE process. Furthermore, the systematic explorations of etching kinetics on Si with ordered nanopatterned Au may further provide an applicable guideline for optimizing the etching conditions and even the desired design strategy on practical applications, particularly in photonic management of Si-based optical devices^{5,6}.

In conclusion, we presented the precise tunability of nanowire dimensions by combining the EBL patterning technique with the MaCE process. The patterned Ti/Au meshes are observed to uniformly sink into Si as catalytic etching proceeds, leaving the aligned nanowire arrays with smooth sidewalls and controllable lengths. The phenomenological model was further applied to elucidate the dependences of the pitch sizes and diameters of metal catalysts on etching kinetics. Notably, the existence of nanogaps (4 nm to 7 nm) between the formed nanowires and surrounding metal meshes provides the diffusion pathway for reactants to reach the metal/Si interfaces. These features on etching sub-100 nm patterns essentially cause the dynamically changed etching process that depends on the spacings of nanogaps. The explicit correlation between etching rates on Si and metal coverage with pitch-varied and diameter-varied patterns validates the proposed series resistance model. These systematic explorations of nanoscale etching on Si, along with the design strategy, are anticipated to benefit practical applications on photonics, sensors, and nanoelectronics.

Acknowledgments

The work is financially supported by Ministry of Science and Technology, Taiwan (MOST 103-2218-E-260-001-).

Notes and references

- 1 Y. Cui and C. M. Lieber, *Science*, 2001, **291**, 851–853.
- 2 X. Zhao, C. M. Wei, L. Yang and M. Y. Chou, *Phys. Rev. Lett.*, 2004, **92**, 236805.
- 3 C. K. Chan, H. Peng, G. Liu, K. McIlwrath, X. F. Zhang, R. A. Huggins and Y. Cui, *Nat. Nanotechnol.*, 2008, **3**, 31–35.
- 4 E. Garnett and P. Yang, *Nano Lett.*, 2010, **10**, 1082–1087.
- 5 G. Bronstrup, N. Jahr, C. Leiterer, A. Csaki, W. Fritzsche and S. Christiansen, *ACS Nano*, 2010, **4**, 7113–7122.

- 6 C. Y. Chen and C. P. Wong, *Chem. Comm.*, 2013, **49**, 7295–7297.
- 7 L. Hu and G. Chen, *Nano Lett.*, 2007, **7**, 3249–3252.
- 8 M. D. Kelzenberg, S. W. Boettcher, J. A. Petykiewicz, D. B. Turner-Evans, M. C. Putnam, E. L. Warren, J. M. Spurgeon, R. M. Briggs, N. S. Lewis and H. A. Atwater, *Nat. Mater.*, 2010, **9**, 239–244.
- 9 X. Li and P. W. Bohn, *Appl. Phys. Lett.*, 2000, **77**, 2572–2574.
- 10 C. Y. Chen, C. S. Wu, C. J. Chou and T. J. Yen, *Adv. Mater.*, 2008, **20**, 3811–3815.
- 11 K. Peng, J. Hu, Y. Yan, Y. Wu, H. Fang, Y. Xu, S. Lee and J. Zhu, *Adv. Funct. Mater.*, 2006, **16**, 387–394.
- 12 C. Y. Chen, W. J. Li and H. H. Chen, *ChemPhysChem*, 2012, **13**, 1415–1420.
- 13 Z. P. Huang, H. Fang and J. Zhu, *Adv. Mater.*, 2007, **19**, 744.
- 14 S. Chang, V. P. Chuang, S. T. Boles and C. V. Thompson, *Adv. Funct. Mater.*, 2010, **20**, 4364.
- 15 J. Kim, Y. H. Kim, S. H. Choi and W. Lee, *ACS Nano*, 2011, **5**, 5242–5248.
- 16 C. Chartier, S. Bastide and C. L. Clement, *Electrochim. Acta*, 2008, **53**, 5509.
- 17 X. Zhong, Y. Qu, Y. C. Lin, L. Liao and X. Duan, *ACS Appl. Mater. Interfaces*, 2011, **3**, 261.
- 18 Z. Huang, X. Zhang, M. Reiche, L. Liu, W. Lee, T. Shimizu, S. Senz and U. Gosele, *Nano Lett.*, 2008, **8**, 3046–3051.
- 19 O. Dietz, H. J. Stockmann, U. Kuhl, F. M. Izrailev, N. M. Makarov, J. Doppler, F. Libisch and S. Rotter, *Phys. Rev. B.*, 2012, **86**, 201106.
- 20 S. K. Srivastava, D. Kumar, S. W. Schmitt, K. N. Sood, S. H. Christiansen and P. K. Singh, *Nanotechnology*, 2014, **25**, 175601.
- 21 M. S. Kulkarni and H. F. Erk, *J. Electrochem. Soc.*, 2000, **147**, 176–188.
- 22 Z. Huang, N. Geyer, P. Werner, J. Boor and U. Gosele, *Adv. Mater.*, 2011, **23**, 285–309.